Tracing the origin and formation mechanisms of coalbed gas from the Fuxin Basin in China using geochemical and isotopic signatures of the gas and coproduced water

Xiangrui Chen[a,b,c], Yunpeng Wang[a,b,*], Mingxin Tao[c], Zheng Zhou[d], Zhihua He[a], Kailin Song[e]

[a] *State Key Laboratory of Organic Geochemistry, Guangzhou Institute of Geochemistry, Chinese Academy of Sciences, Guangzhou 510640, China*

[b] *CAS Center for Excellence in Deep Earth Science, Guangzhou 510640, China*

[c] *Faculty of Geographical Science, Beijing Normal University, Beijing 100875, China*

[d] *Lancaster Environment Centre, Lancaster University, Lancaster LA1 4YQ, UK*

[e] *Liaoning Energy Geological Exploration and Development Research Institute Co., Shenyang 110003, China*

*Corresponding author. Email: wangyp@gig.ac.cn

Abstract

Coalbed gas (CBG) is an unconventional natural gas with a large resource potential. In order to determine its origins, formation pathways and mechanisms, studies on the geochemistry of CBG, coalbed water and coal have been carried out for years. However, the relationship between geochemistry of CBG and coalbed water is still not clear, especially with respect to the CO_2 dissolution process. Here, a comprehensive study on

the geochemistry of CBG and coproduction water in samples from the Fuxin Basin, China, is presented. Twenty-four gas and water samples were collected directly from the CBG producing well heads. $C_1/(C_2 + C_3)$ values are far greater than 1000, $\delta^{13}C_1$ values range between -62.8 and -57.6‰, δD_{CH4} values are from -252 to -225‰, $\Delta D_{H2O\text{-}CH4}$ values are from 148 to 178‰, and $\alpha_{CO2\text{-}C1}$ values are from 1.04 to 1.05. The composition characteristics, associated with the genetic diagrams of $\delta^{13}C_1$ vs. δD_{CH4} and $\delta^{13}C_1$ vs. $\delta^{13}C_{CO2}$, and low coal rank (0.4-0.6% Ro), suggest that the CBG in the Fuxi Basin is mainly microbial gas. The Na-HCO_3-Cl type of water in the coalbed is favorable for methanogenesis. δD_{H2O} and $\delta^{18}O_{H2O}$ plot along the global meteoric water line (GMWL) and to the left of the local meteoric water line (LMWL), suggesting that the coalbed water is mainly from meteoric water recharge. However, isotope values in water may have been modified by methanogenesis and water-rock interaction. $\Delta D_{H2O\text{-}CH4}$ values of 148 to 178‰ suggest that methanogenic pathway is mainly CO_2 reduction. However, $\alpha_{CO2\text{-}C1}$ values of 1.04 to 1.05 suggest that methanogenesis pathway might be acetoclastic or methylotrophic. This inconsistency may be caused by low $\delta^{13}C_{CO2}$ values (-19.2 to -14.2‰) and thus low $\alpha_{CO2\text{-}C1}$ values due to high dissolution effect of CO_2 and relative strong hydrodynamic activity in coal aquifers in the Fuxin Basin. Groundwater flow can carry away ^{13}C-enriched CO_2 dissolved in water, thus, the residual CO_2 and DIC are depleted in ^{13}C. Consequently, CO_2 reduction is likely the main methanogenic pathway in the basin. Although CH_4 and H_2O may be close to isotope equilibrium for some samples, the CH_4, CO_2 and HCO_3^- are isotopically in disequilibrium at present reservoir conditions. Overall, kinetic processes largely control isotopic composition and distribution of the CBG and coalbed water in the Fuxin Basin. The CBG in the Fuxin Basin has been continuously generated, probably since the deposition of the coal-bearing formation. Although part of the CBG may have been lost

during coalbed uplift stage, uplift to near surface allow re-inoculation of coalbeds with methanogenic microbial consortia via meteoric water recharge, which can accelerate the formation and accumulation of the microbial CBG. Consequently, most CBG in the present coalbed has been generated likely after the coal strata uplift.

Keywords: Microbial coalbed gas; Coproduction water; CO_2 dissolution; Isotope fractionation; Fuxin Basin

1. Introduction

Coalbed gas (CBG) is an important energy resource and a potential source of greenhouse gas. The estimated global reserves of CBG are 50 trillion m^3, equivalent to 11% of conventional natural gas resources (Mayumi et al., 2016). CBG emissions account for about 10% of global atmospheric inputs of this greenhouse gas (Lloyd et al., 2021). Therefore, efficient development of CBG is of major significance in energy supply and control of greenhouse gas emission.

CBG have microbial, thermogenic, and mixed origins (Scott et al., 1994, Tao et al., 2007; Strąpoć et al., 2011). The microbial gas includes primary and secondary microbial (biogenic) gas. The thermogenic gas can be classified as the thermal degradation gas and thermal cracking gas (Tao et al., 2020, 2021). The mixed CBG often consists of secondary microbial gas and thermal degradation gas (Tao et al., 2007, 2015; Golding et al., 2013). Identifying the origins, formation pathways and mechanisms of CBG is important for formulating effective CBG exploration and

development strategies, as well as enhancing microbial coalbed methane (Park and Liang, 2016).

The isotopic composition of natural gas can, to a significant extent, record their formation processes and mechanisms (Whiticar et al., 1986; Milkov and Etiope, 2018; Xie et al., 2021). Empirical isotope proxies (such as, $\delta^{13}C_1$, δD_{CH4}, $\delta^{13}C_2$, $\delta^{13}C_3$, $\delta^{13}C_{CO2}$, $\delta^{13}C_1$ vs. δD_{CH4}, $\delta^{13}C_1$ vs. $\delta^{13}C_{CO2}$) have been used frequently for tracing the origins, thermal evolution degrees and migrations of natural gas (Schoell, 1980; Chung et al., 1988; Whiticar, 1999; Dai et al., 2018; Liu et al., 2019). These tracers were mainly developed from studying conventional natural gas, and applied to CBG as an extension (Strąpoć et al., 2007; Tao et al., 2021). However, compared to conventional natural gas, CBG has its own features. For example, it experiences adsorption and desorption processes with less migration, and the burial depth is shallow (typically < 2000m). The difference between conventional and unconventional gases can cause uncertainties in applying empirical geochemical indicators to CBG (Tao et al., 2007, 2021; Bates et al., 2011; Vinson et al., 2017). For example, the CBG from the eastern Surat Basin was thermogenic or mixed gas based on the $\delta^{13}C_1$ indicator, however, other geochemical indicators suggested that the CBG was dominated by microbial gas (Hamilton et al., 2014). Plotting δD_{CH4} vs. $\delta^{13}C_1$ for the CBG from the Powder River Basin indicated that the main methanogenic pathway was acetate fermentation. But, the $\Delta^{13}C_{CO2\text{-}CH4}$ indicator suggested that the majority of methane had been generated via CO_2 reduction (Flores et al., 2008). Bates et al. (2011) proposed that the $\delta^{13}C$ values of CH_4 and CO_2 could indicate the extent of

methanogenesis (i.e., early versus late stage), rather than the dominant methanogenic pathways. Milkov and Etiope (2018) updated the commonly used three genetic diagrams of natural gas ($C_1/(C_2 + C_3)$ vs. $\delta^{13}C_1$, $\delta^{13}C_1$ vs. δD_{CH4}, $\delta^{13}C_1$ vs. $\delta^{13}C_{CO2}$) using geochemical and geological data from > 20,000 biotic and abiotic natural gas samples. However, the revision could not distinguish the formation pathways of secondary microbial methane. Previous studies showed that many factors or processes could significantly change the isotopic compositions and distributions of CBG (Scott et al., 1994; Vinson et al., 2017; Tao et al., 2021). For example, isotopic desorption fractionation and mixing between secondary microbial and thermogenic gas often made isotopic compositions of CBG more variable and complex (Tao et al., 2007, 2021). Anaerobic methane oxidation, sulfate reduction, and CO_2 dissolution can also affect the isotopic compositions of CBG (Vinson et al., 2017). Thus, uncertainties remain when directly applying the empirical isotope indicators developed from studying conventional natural gas to CBG.

Since 1994, coalbed water geochemistry has also been used to constrain origins, formation pathways and migrations of CBG (Scott et al., 1994; Zhou et al., 2005; Sharma and Baggett, 2011; Golding et al., 2013). Many studies have shown that groundwater from coalbeds containing microbial gas is typically Na-HCO_3 or Na-HCO_3-Cl type of water with high alkalinity and modest pH values between 6 and 9 (Golding et al., 2013). The δD_{H2O} and $\delta^{18}O_{H2O}$ generally plot along the global meteoric water line (GMWL) (Kinnon et al., 2010; Schlegel et al., 2011; Baublys et al., 2015). The $\delta^{13}C$ value of dissolved inorganic carbon (DIC) has been suggested as

a new tracer for distinguishing microbial CBG. Coalbed water with $\delta^{13}C_{DIC}$ significantly enriched in ^{13}C usually suggests that the corresponding CBG contains microbial methane (Golding et al., 2013). For example, the microbial CBG was found in the Alberta, the Illinois, the Surat, and the Cesar Rancheria Basins; where the average $\delta^{13}C_{DIC}$ is 22.5‰ in the Alberta Basin (Harrison et al., 2006), greater than 12.6‰ in the Illinois Basin (Schlegel et al., 2011), greater than 10‰ in the Surat Basin (Baublys et al., 2015), and greater than 6‰ in the Cesar Rancheria Basin (Castaneda et al., 2022), respectively.

Currently, the relationship between geochemistry of CBG and coalbed water is still not clear, especially for the coupling relationship of CO_2 and DIC. Although CO_2 has high solubility at geological conditions (Akinfiev and Diamond, 2010; Mao et al., 2013), and solubility trapping in formation water is likely the dominant CO_2 sink (Gilfillan et al., 2009), the dissolution effect of CO_2 is often ignored, making isotopic indicators referring to CO_2 likely unreliable. In order to reliably distinguish CBG origins and formation mechanisms, a systematic study on the geochemical compositions of CBG, coalbed water and coal is necessary in addition to studying CBG geochemistry alone. The Fuxin Basin is an important coal and CBG production area in the northeast China. The coal-bearing strata are relatively young, and the reservoirs are favorable for conservation of CBG (Zhu et al., 2007), providing ideal conditions for studying the coupling relationship of CBG and coalbed water geochemistry. We collected 24 CBG and coproduction water samples from the Fuxin basin for this study. The geochemistry data of the related coals are obtained from the

CBG production unit. A comprehensive study on the geochemical compositions and variations, origins and formation mechanisms of the Fuxin CBG and coalbed water is presented.

2. Geological setting

The Fuxin Basin is located in the western Liaoning Province, China. It is 11-22km wide, 80km long and covers an area of 1,500km^2 (Zhu et al., 2007). The commercial CBG extraction in the basin began in 1999. The basin is a NE-NNE-trending graben basin with the Pre-Mesozoic basement overlain by the Cretaceous cap rocks (Fig. 1). Its formation and evolution are controlled by the eastern Lüshan and western Songling faults (Zhu et al., 2007). The structural units of the basin include the western step-fault zone, the Xinqiu, the Haizhou, the Yimatu, and the Minjiatun subsags; the Shibei, the Yixian, and the Minnan slope zones; the Fuxin, the Dongliang, and the Qinghemen-Aiyou tectonic zones (Fig.1a) (Jia et al., 2021).

The basin was filled with early Cretaceous volcanic and terrigenous sedimentary strata (130-100Ma) (Fig. 1b) (Wang et al., 2007; Jia et al., 2021; Zhang et al., 2021). The strata comprise the Yixan (K_{1y}), Jiufotang (K_{1jf}), Shahai (K_{1sh}), Fuxin (K_{1f}), and Sunjiawan (K_{1s}) Formations (Figs. 1b and 1c). The K_{1y} is characterized by volcanic rocks. The K_{1jf} is mainly composed of tuff, conglomerate, sandstone and mudstone. The K_{1sh} is mainly composed of sandy conglomerate, mudstone and sandstone, interbedded with siltstone and coal seams. The K_{1f} is mainly composed of sandstone, siltstone, mudstone, and conglomerate interlayered with multiple coal seams. The K_{1f} is the primary coal-bearing strata in the basin. During the deposition of K_{1f} (113-107Ma), the regional tectonic stress field began to change from transtension to

transpression, which caused a rapid deposition of 444.5m/Ma (Zhu et al., 2007). This is favorable for the coal and CBG formation and conservation. The K_{1s} consists of sandy conglomerate and sandstone, interlayered with siltstone and mudstone.

Samples in this study are collected in the Haizhou subsag (Fig. 1a). In the subsag, the coalbeds include the Shuiquang, the Sunben, the Middle, the Taiping, and the Gaode coalbeds (Zhu et al., 2007). The target coalbeds for CBG development are the Sunben, the Middle and the Taiping coalbeds. They have stable distribution in the whole study area. Their average thicknesses are 15.1m, 9.4m, and 10.4m, respectively (Xie, 2020). The three target coalbeds are aquifers, and the over- and under-lying strata are aquitards. The natural fractures and near-surface location of the coalbeds in the eastern basin can induce modern meteoric recharge. The groundwater in the coalbed aquifers flow from the east to central section. There are two main normal faults in the area. They are not favorable for CBG conservation. The coal rank is subbituminous. Coal macerals consist of 83.3 to 97.6% vitrinite, 0.2 to 11.8% inertinite, and < 5% liptinite (Xie, 2020).

3. Methods

3.1 Sampling

24 CBG and coproduction water samples were collected directly from the CBG producing well heads. Gas and water samples were collected in 250ml glass bottles. Gas samples were collected in inverted bottles by displacement of saturated NaCl solution. The volume of gas is about one third of the bottle volume. Water samples were filtered via glass fiber filter membranes and collected in glass bottles without headspace. Before sampling, these bottles were flushed three times repeatedly with

coalbed water.

3.2 Analytical methods

Geochemical composition of gas samples and concentrations of inorganic ions in water samples were analyzed at Guangzhou Institute of Geochemistry, Chinese Academy of Sciences. The isotope compositions of water samples were measured at the Beijing LICA United Technology Ltd.

The molecular components of the gas samples were measured by an Agilent 8890 gas chromatograph (GC). A PoraPLOT Q capillary column (30m×0.25mm×0.25μm) was used with helium as carrier gas. The GC oven was held isothermally at 70°C for 6 mins and programmed to increase to 180°C at a rate of 15°C/min, and then to hold for 4mins. The relative error of the results was < 0.5%.

The carbon and hydrogen isotope compositions of gas samples were measured on a Gas Chromatograpy-Isotope Ratio Mass Spectrometry (GC-IRMS). A 6890N gas chromatograph installed with CP-Poraplot Q column (30m×0.32mm×0.25μm) was used with helium as carrier gas. The conditions were initially held at 50ºC for 3mins, then heated to 190ºC at a rate of 15ºC/min and held for 7mins. Carbon isotopes were measured using a Isoprime 10 IRMS and are reported relative to Vienna Pee Dee Belemnite (VPDB). Before and after each gas sample analysis, a CO_2 gas standard was used to calibrate the instrument. The errors were less than ±0.3‰. Hydrogen isotopes were measured using a Trace 1310-Delta V Advantage IRMS, and are reported relative to Vienna Standard Mean Ocean Water (VSMOW) with a precision of ±3‰.

The oxygen and hydrogen isotope compositions of water samples were measured on a Liquid Water Isotope Analyzer (GLA431-TLWIA), and are reported relative to

VSMOW with precision of ±1‰ for hydrogen and ±0.2‰ for oxygen. The GLA431-TLWIA is based on the Off-axis Integrated Cavity Output Spectroscopy. The carbon isotope ratios of DIC from coalbed water samples were analyzed on a Finnigan MAT 253, and reported relative to VPDB with precision of ±0.2‰. Samples were pretreated by injecting pure phosphoric acid to acquire CO_2 (Li et al., 2007).

The pH values of water samples were measured at the sampling site. Total dissolved solids (TDS) of the water samples were measured by weighing the residues after waters were evaporated to dryness. Alkalinities as bicarbonate concentration (mg/L) were measured by the H_2SO_4 titration method using a TitroLine Easy Schott automatic titrator (Lico et al., 1982; Chen et al., 2018). Samples with volumes of 30mL were titrated to a pH of 2.5 with 0.1mol/L H_2SO_4 solution, and the alkalinities were calculated from the amount of acid used to reach the endpoints in the titration curves. Replicated analysis yielded a maximum 5% error. The ion concentrations were analyzed by ion chromatography following appropriate dilution (10 or 100 times) with a Dionex ICS900 instrument. The major anions (Cl^-, F^-, SO_4^{2-}) were separated within an IonPac AS15 column and determined by a DS5 conductivity cell. The eluent was 5 mM KOH solution. The major cations (Na^+, K^+, Ca^{2+}, Mg^{2+}) were separated within an IonPac CS12A ion exchange column and determined by a DS5 conductivity cell. The eluent was 18mM methanesulfonic acid. The relative analytical uncertainties were better than 5.0%.

4. Results and discussion

4.1 Molecular and isotopic compositions of CBG in the Fuxin Basin

In gas samples, CH_4 is the predominant component with concentrations ranging

from 91.93 to 94.51% (Table 1). Another main component is N_2, with concentrations of 5.2 to 7.68%. CO_2 concentrations are from 0.12 to 0.5%. The ratios of CH_4/CO_2 are from 186 to 776. C_{2+} hydrocarbon gas concentrations are below measurement limit (< 0.01%). Therefore, $C_1/(C_2 + C_3)$ ratios are far greater than 1000, indicating the CBG in the Fuxin Basin are dry gas. In general, dry gas with $C_1/(C_2 + C_3) > 1000$ is the characteristic of microbial gas, late mature thermogenic gas, and/or abiotic gas (Milkov and Etiope, 2018). For our CBG samples, their sources and reservoirs are coalbeds, they are unlikely abiotic gas. The source coal is subbituminous with low Ro of 0.40 to 0.60%, indicating that these samples are not late mature thermogenic gas. Hence, the CBG in the Fuxin Basin is likely microbial in origin.

In the CBG samples, $\delta^{13}C_1$ values are from -62.8 to -57.6‰, δD_{CH4} values are from -252 to -225‰, and $\delta^{13}C_{CO2}$ values are from -19.2 to -14.2‰ (Table 1). Fractionation factor $\alpha_{CO2\text{-}C1}$ ($\alpha=(1000+\delta^{13}C_{CO2})/(1000+\delta^{13}C_1)$) are from 1.04 to 1.05. Binary genetic diagrams of $\delta^{13}C_1$ vs. δD_{CH4} and $\delta^{13}C_{CO2}$ vs. $\delta^{13}C_1$ are important tools for distinguishing origin of natural gases (Whiticar, 1999; Milkov and Etiope, 2018). In the genetic diagrams (Figs. 2a and 2b), isotopic data of the CBG samples fall in the common zone of microbial and thermogenic gas. Regardless of primary or secondary microbial gas, the two genetic diagrams show that the CBG in the Fuxin Basin could be microbial, thermogenic, or mixed gas (Fig. 2). However, the correlation of $\delta^{13}C_1$ and δD_{CH4} in the samples is extremely low with a correlation coefficient r^2 of only 0.0002 (Fig. 3). This characteristic suggests that the CBG is not thermogenic, because the δD_{CH4} of thermogenic CBG often increases with increasing $\delta^{13}C_1$ (Milkov and Etiope, 2018; Tao et al., 2020). $\alpha_{CO2\text{-}C1}$ values between 1.04 and 1.05 also suggest that the CBG samples are unlikely thermogenic gas, because the $\alpha_{CO2\text{-}C1}$ value of thermogenic gas is generally less than 1.03 (Whiticar, 1999; Golding et al., 2013). All

evidence indicates that the Fuxin CBG is mainly microbial gas.

4.2 Chemical and isotopic compositions of coalbed water

The pH values of water samples are from 8.08 to 8.46. The TDS concentrations are from 545 to 1418mg/L (Table 2). Waters with TDS values < 1500mg/L are regarded as fresh, while waters with TDS values between 1500 and 35,000mg/L are thought to be brackish (Baublys et al., 2015). Using this classification, coalbed water in the Fuxin Basin is fresh water. The coalbed water is of Na-HCO_3-Cl type (Fig. 4, Table 2). The cation concentrations of Na^+, Ca^{2+} and Mg^{2+} are from 473.4 to 700.3mg/L, 34.9 to 117.6mg/L, and 4.6 to 13.5mg/L, respectively; the anion concentrations of HCO_3^-, Cl^- and SO_4^{2-} are from 1244.4 to 1464.0mg/L, 181.1 to 231.8mg/L, and 7.9 to 14.8mg/L, respectively (except for sample FX-11) (Table 2). The low concentrations of SO_4^{2-} and TDS are favorable for methanogenesis.

[Ca^{2+}]/[Mg^{2+}] ratios are from 1.9 to 11.0, indicating a relative enrichment of Ca^{2+} in the water samples. Plot using Na-normalized molar ratio of Ca/Na vs. Mg/Na (Fig. 5) is an important tool in distinguishing the source rocks of Ca^{2+} and Mg^{2+} in groundwater (Gaillardet et al., 1999, Li et al., 2016). Fig. 5 shows that Ca and Mg cations in the water samples mainly originate from the dissolution of evaporites. [Mg^{2+}+Ca^{2+}]/[HCO_3^-] ratios are low from 0.06 to 0.17. The extra HCO_3^- may also promote Ca^{2+} and Mg^{2+} precipitation in coal-bearing formations (Van Voast, 2003).

HCO_3^- in coalbed water mainly originates from dissolution of carbonates and/or breakdown of organic matter (Sharma and Baggett, 2011; Golding et al., 2013). The dissolution of carbonates can lead to relative high concentrations of Ca^{2+}+Mg^{2+} and HCO_3^- in groundwater (Van Voast, 2003). In the Fuxin Basin, formations lack carbonate rocks, and the coalbed water is Na-HCO_3-Cl type with low

288 $[Mg^{2+}+Ca^{2+}]/[HCO_3^-]$ values of 0.06 to 0.17. These characteristics suggest that the
289 high concentrations HCO_3^- in the water samples unlikely originate from dissolution of
290 carbonates. In addition, many studies have shown that DIC (whose dominant
291 composition is HCO_3^-) in the coproduction water of microbial CBG are mainly from
292 CO_2 dissolution (Golding et al., 2013). Gilfillan et al. (2009) also suggest that
293 solubility trapping in formation water is the dominant CO_2 sink. Hence, the HCO_3^- in
294 water samples may primarily originate from the dissolution of CO_2 generated during
295 microbial CBG formation.

296 The δD_{H2O} and $\delta^{18}O_{H2O}$ values of water samples are from -83.6 to -73.9‰, and
297 from -12.1 to -10.1‰, respectively (Table 1). They plot along the GMWL (Fig. 6a)
298 and to the left of the local meteoric water line (LMWL) (except for sample FX-6)
299 (Fig. 6b). Due to lack of monitoring for isotope composition of the precipitation in the
300 Fuxin Basin, the LMWL was based on the monitoring results from Northeast China
301 meteoric water isotope monitoring network. The LMWL equation is from Wang et al.
302 (2016)

303 $$\delta D_{H2O} = 7.27\delta^{18}O_{H2O} - 1.54 \quad (n=111,\ r=0.97). \tag{1}$$

304 In sedimentary basins, groundwaters with isotopic compositions to the right of the
305 GMWL are common (Golding et al., 2013), because many processes, such as
306 evaporation, mixing with seawater or basinal brines, and fluid-rock interaction under
307 high temperature conditions, can shift meteoric water compositions to the right of the
308 GMWL (Clayton et al., 1966; Taylor, 1997). However, coalbed waters, especially
309 associated with microbial CBG, typically plot along and to the left of the GMWL, e.g.
310 coalbed waters from the Elk Valley coalfield (Aravena et al., 2003), the Bowen Basin
311 (Kinnon et al., 2010), the Powder River Basin (Bates et al., 2011), the Illinois Basin
312 (Schlegel et al., 2011), and the Surat Basin (Baublys et al., 2015) (Fig. 6a). The

distribution characteristics suggest that the coalbed waters are mainly from the meteoric water recharge, however, their isotope compositions may have been affected by methanogenesis and water-rock interaction under low temperature conditions (Golding et al., 2013).

Methanogenesis can lead to isotopic compositions of groundwaters to the left of the GMWL or LMWL because methanogens preferentially use water-derived hydrogen that enriches the residual water in deuterium (Golding et al., 2013). Especially for hydrogenotrophic methanogenesis, the effect is much great, because all four hydrogen atoms in methane molecule are derived from the water molecules (Whiticar, 1999). For our samples, $\Delta D_{H2O\text{-}CH4}$ are from 148 to 178‰, suggesting that the dominated methanogenesis pathway is hydrogenotrophic (Golding et al., 2013). The isotope values of water samples plotting to the left of the LMWL (Fig. 6b) likely has been affected by methanogenesis. In addition, other processes, such as precipitation of carbonates and clays in coal cleats and alteration of feldspars and lithics in interburden sandstones, can also lead to the water samples depleted in ^{18}O and enriched in D (Kinnon et al., 2010; Golding et al., 2013), thus, the isotope data fall to the left of the LMWL.

Overall, the isotopic distribution characteristics of coalbed water samples (Fig. 6), associated with their low TDS, suggest that the Fuxin coalbed waters are mainly from the meteoric water recharge. However, their isotope values may have been modified by methanogenesis and water-rock interaction.

4.3 Inconsistency of isotope indicators in distinguishing methanogenic pathways

Microbial conversion of coal into methane is a multi-step process. Currently only the final step for the methanogenesis is partially understood, namely, methanogenesis

pathways are hydrogenotrophic (CO_2 reduction), acetoclastic, and methylotrophic, as shown in the following reactions:

$$CO_2 + 4H_2 \rightarrow CH_4 + 2H_2O \quad (2)$$

$$CH_3COOH \rightarrow CH_4 + CO_2 \quad (3)$$

$$CH_3X + H_2O \rightarrow CH_4 + X' - H \quad (4)$$

where the CH_3X covers a range of methy-bearing compounds, such as methanol, methylamine and methyl sulfide (Park and Liang, 2016).

Isotope techniques have been used to constrain methanogenic pathways in the reactions (2-4). The quantitative relationship of δD values of methane and coexisting water can be employed to constrain methanogenic pathways. For CO_2 reduction to CH_4, the empirical relationship between δD_{CH4} and δD_{H2O} is

$$\delta D_{CH_4} = \delta D_{H_2O} - \beta. \quad (5)$$

Where β ranges from 150 to 170‰ (Schoell, 1980). However, Whiticar (1999) proposed that β ranges from 160 to 180‰. Statistical analysis of previous studies shows that, in CBG fields where methanogenesis is dominated by CO_2 reduction, the majority of $\Delta D_{H2O\text{-}CH4}$ values fall within the range of 150-180‰ (Fig. 7), such as in the Bowen Basin (Kinnon et al., 2010), the Powder River Basin (Bates et al., 2011), the Illinois Basin (Schlegel et al., 2011), the Surat Basin (Baublys et al., 2015), and the Cesar Rancheria Basin (Castaneda et al., 2022). The $\Delta D_{H2O\text{-}CH4}$ value is less than 130‰ for the thermogenic CBG from the Qinshui Basin (Xu et al., 2016) (Fig. 7). In general, $\Delta D_{H2O\text{-}CH4}$ values associated with acetate or methylated substrate fermentation are significantly larger than those associated with CO_2 reduction

(Whiticar et al., 1986; Whiticar, 1999). Thus, current literature studies indicate that the difference in hydrogen isotope in the equation (5) varies from 150 to 180‰. In Fuxin samples, δD_{CH4} and δD_{H2O} values are from -252 to -225‰ and from -83.6 to -73.9‰, and $\Delta D_{H2O\text{-}CH4}$ values are from 148 to 178‰ (Fig. 7, Table 1). These composition characteristics suggest that CO_2 reduction is the dominant methanogenic pathway in the Fuxin Basin.

Fractionation factor $\alpha_{CO2\text{-}C1}$ is also often employed to infer methanogenic pathways. The $\alpha_{CO2\text{-}C1}$ values for CO_2 reduction and fermentations of acetate or methylated substrates are generally between 1.05 (or 1.06) and 1.09, and between 1.03 (or 1.04) and 1.06, respectively (Whiticar, 1999; Golding et al., 2013). In Fuxin samples, $\alpha_{CO2\text{-}C1}$ values are from 1.04 to 1.05, suggesting that the methanogenesis pathway is mainly acetoclastic or methylotrophic (Fig. 8).

For the Fuxin CBG samples, $\alpha_{CO2\text{-}C1}$ and $\Delta D_{H2O\text{-}CH4}$ indicators are inconsistent in distinguishing methanogenic pathways. We find that the $\delta^{13}C_1$ and $\Delta D_{H2O\text{-}CH4}$ values of samples from the Fuxin Basin are consistent with those from other microbial CBG basins (such as, the Powder River Basin, the Illinois Basin, the Surat Basin, and the Cesar Rancheria Basin), however, the $\delta^{13}C_{CO2}$ values from the Fuxin Basin are significantly lower than those from other basins (Table 3, Fig. 9). The normal $\delta^{13}C_1$ values and low $\delta^{13}C_{CO2}$ values can lead to low $\alpha_{CO2\text{-}C1}$ values. In fact, in CBG formation and evolution processes, a number of processes can significantly affect $\delta^{13}C_1$, $\delta^{13}C_{CO2}$ and therefore $\alpha_{CO2\text{-}C1}$, including mixing between microbial and thermogenic CBG, extent of methanogenesis relative to non-methanogenic processes,

anaerobic methane oxidation, and dissolutions of gas CO_2 and carbonate minerals.

In general, $\alpha_{CO2\text{-}C1}$ value of microbial gas is greater than that of thermogenic gas, which typically exhibits more positive $\delta^{13}C_1$ and more negative $\delta^{13}C_{CO2}$. Thermogenic-microbial mixing would reduce $\alpha_{CO2\text{-}C1}$ values. However, from the analysis above, the Fuxin CBG is mainly microbial in origin. A small amount of thermogenic CBG formed in the basin would not significantly affect the $\alpha_{CO2\text{-}C1}$ values. Non-methanogenic processes, such as sulfate and iron reduction, can produce CO_2 whose $\delta^{13}C$ value is much lower than that of the CO_2 formed in methanogenesis. If CO_2 in Fuxin CBG samples originated from both sulfate and/or iron reduction and methanogenesis, $\alpha_{CO2\text{-}C1}$ values would be lower than that in the methanogenic gas. However, sulfate reduction usually occurs in shallow methanogenic environments and the SO_4^{2-} concentrations generally exceed 10mM (Rice and Claypool, 1981; Mitterer, 2010; Li et al., 2016). For Fuxin samples, the burial depths of CBG are still deep (>1000m) after the uplift of coalbed, and SO_4^{2-} concentrations are less than 0.15mM. Sulfate reduction may have occurred in the early stage of Fuxin CBG formation, but it is weak after the uplift of coalbed. Iron reduction is less likely to produce a large proportion of CO_2 due to its low content in the Fuxin coal strata. Anaerobic methane oxidation could shift the residual CBG to higher values of $\delta^{13}C_1$ and lower values of $\delta^{13}C_{CO2}$, thus lower values of $\alpha_{CO2\text{-}C1}$ (Whiticar et al., 1986). For Fuxin samples, although their $\delta^{13}C_{CO2}$ values are significantly lower than the $\delta^{13}C_{CO2}$ values from other microbial CBG basins, their $\delta^{13}C_1$ values are consistent with the $\delta^{13}C_1$ values from these basins (Fig. 9). Therefore, anaerobic methane oxidation may not

404 significantly affect $\alpha_{CO2\text{-}C1}$ values. From chemical analysis of water, dissolution effect
405 of carbonate mineral is weak in the Fuxin coal-bearing strata. It cannot significantly
406 affect the $\alpha_{CO2\text{-}C1}$ values.

407 Dissolution of CO_2 can reduce apparent $\alpha_{CO2\text{-}C1}$ values, because its dissolution can
408 result in enrichment of ^{13}C in dissolved CO_2 (Martini et al., 2003; Bates et al., 2011).
409 CO_2 dissolution is likely an important reason for the low $\delta^{13}C_{CO2}$ values in Fuxin
410 CBG. The evidence suggests that at least some of the CO_2 dissolved into groundwater
411 to form DIC during microbial CBG formation. Culture experiments for coal
412 conversion to methane have found that coals can produce comparable amounts of
413 microbial CH_4 and CO_2. For example, Zhang et al. (2015) carried out culture
414 experiments using bituminous coal as sole carbon source and the microorganisms
415 from the CBG coproduction waters from the Illinois Basin, USA. Rate of CH_4 yield
416 was 0.159m^3/ton/day in 20 days, and rate of CO_2 yield was 0.174m^3/ton/day in the
417 first 10 days. Rathi et al. (2019) carried out similar culture experiments. The water
418 and coal samples were collected from a CBG well in the Jharia block, India. After six
419 enrichment cycles, 1002μmol CH_4/g coal and 629μmol CO_2/g coal were detected. The
420 yield ratio of CH_4/CO_2 is 1.59. Culture experiments using anthracite coal and water
421 samples from the Qinshui Basin, China were carried out by Xiao et al., 2013. The
422 average yield ratios of CH_4/CO_2 for the Fm 3# and Fm 15# coal samples are 1.08 and
423 1.75, respectively. However, microbial CBG from *in situ* coalbeds are often enriched
424 in CH_4 (>70%), but significantly depleted in CO_2 (typically <10%). Gas dissolution
425 effect may interpret the inconsistence of CH_4/CO_2 in culture experiment and field-

collected samples. The solubility of CO_2 is several times higher than that of CH_4 under certain temperature, pressure and salinity conditions (Fig. 10) (Duan et al., 1992; Akinfiev and Diamond, 2010). In relatively high-pressure and enclosed CBG reservoirs, high CO_2 solubility and low CH_4 solubility can cause low CO_2 content and high CH_4 content in CBG. However, their dissolution effects may be weak in culture experiments due to low-pressure conditions and short experiment period. Since large amounts of water are often produced in CBG recovery (Hamawand et al., 2013; Meng et al., 2014), coalbeds can also contain large amounts of dissolved CO_2. In addition, as previously stated, the HCO_3^- (DIC) in Fuxin water samples mainly originated from the CO_2 dissolution and, compared with TDS concentrations in CBG coproduction waters from other microbial CBG basins, the TDS concentrations in Fuxin water samples are significantly lower (Table 3), suggesting that the hydrodynamic activity in Fuxin coalbed aquifers is much stronger. Rapid groundwater flow can carry away ^{13}C-enriched dissolved CO_2 (Vinson et al., 2017), thus, the residual CO_2 and DIC are depleted in ^{13}C in Fuxin gas and water samples (Table 3).

Biological, thermochemical, and chemical processes have been considered for the conversion of coal to valuable chemicals. We propose that CO_2 dissolution and strong hydrodynamic activity in Fuxin coalbed aquifers are two important reasons for low $\delta^{13}C_{CO2}$ values and thus low $\alpha_{CO2\text{-}C1}$ values in Fuxin CBG samples. Hence, the inconsistency of $\alpha_{CO2\text{-}C1}$ and $\Delta D_{H2O\text{-}CH4}$ indicators for the samples may be due to low $\delta^{13}C_{CO2}$ values. Consequently, $\Delta D_{H2O\text{-}CH4}$ indicator is more suitable than $\alpha_{CO2\text{-}C1}$ indicator, thus, CO_2 reduction is likely the primary methanogenic pathway in the

Fuxin Basin.

4.4 Kinetic vs. equilibrium isotope fractionations of gas and water in the Fuxin Basin

There is ongoing debate concerning whether it is the kinetic or equilibrium mechanism that controls isotopic composition and formation of natural gas (Stolper et al., 2014; Wang et al., 2015; Thiagarajan et al., 2020). By comparing isotopic equilibrium temperatures and CBG formation temperatures, it is possible to evaluate the importance of equilibrium or kinetic effect in controlling the isotopic composition and formation of the CBG in the Fuxin Basin (Turner et al., 2021).

In the CBG production zone of the Fuxin Basin, the measured formation temperatures are between 28.0°C and 35.5°C at the depth of 1050m, and the average geothermal gradient is 2.5°C/hm. Assuming the temperature at 1050m depth is 31.75°C (average of 28.0°C and 35.5°C), the burial depths of the CBG are from 1300 to 1700m, the estimated reservoir temperatures are between 38°C and 48°C.

Typical carbon and hydrogen isotopic exchange reactions for isotopic equilibriums among CH_4, CO_2, H_2O and HCO_3 can be written as

$$^{12}CO_2 + {}^{13}CH_4 \leftrightarrow {}^{13}CO_2 + {}^{12}CH_4 \quad (6)$$

$$H_2O + CH_3D \leftrightarrow HDO + CH_4 \quad (7)$$

$$H{}^{12}CO_3^- + {}^{13}CO_2 \leftrightarrow H{}^{13}CO_3^- + {}^{12}CO_2 \quad (8)$$

$$H{}^{12}CO_3^- + {}^{13}CH_4 \leftrightarrow H{}^{13}CO_3^- + {}^{12}CH_4 \quad (9)$$

Chen et al. (2019) provided a method to calculate the equilibrium constants for the reaction (6). Their calculated results were consistent with other theoretical and experimental results (Richet et al., 1977; Horita, 2001; Kueter et al., 2019; Turner et al., 2021). The code developed in the MatLab software from Chen et al.

(2019) was used to calculate the equilibrium temperature T_1 in the reaction (6). The equation from Turner et al. (2021) was used to calculate the equilibrium temperature T_2 of the reaction (7). The calculated T_1 are from 112 to 147°C, and the T_2 are from 3 to 50°C (except for sample FX-11) (Fig.11, Table 4).

According to experimental data from Mook et al (1977), when reaction (8) is in equilibrium, the difference of $\Delta^{13}C$ (HCO_3^--CO_2) is approximately 10.1‰ at 5°C. And $\Delta^{13}C$ (HCO_3^--CO_2) value decreases with increasing temperature in the range of 0 to 100°C. In Fuxin samples, the $\Delta^{13}C_{DIC\text{-}CO2}$ values are greater than 10.1‰. Because $\delta^{13}C_{HCO3-}$ values are approximate to $\delta^{13}C_{DIC}$ values, the $\Delta^{13}C$ (HCO_3^--CO_2) values are also greater than 10.1‰. Thus, the equilibrium temperature T_3 of the reaction (8) is less than 5°C (Table 4).

We applied the relationships of equilibrium constants of reactions (6, 8, 9) to judge whether the calculated equilibrium temperature T_4 of the reaction (9) is consistent with CBG reservoir temperature. Given the reaction (8) is in equilibrium at 43°C (average of reservoir temperatures), the $\delta^{13}C_{CO2}$ value is approximately -5.3‰ when the $\delta^{13}C_{DIC}$ value is 0.81‰ (average of samples). If CO_2 with $\delta^{13}C$ of -5.3‰ is in equilibrium with CH_4 with $\delta^{13}C$ of -60.0‰ (average of samples), the calculated equilibrium temperature T_4 is 71°C, which is higher than the average reservoir temperature of 43°C.

As a result, the calculated T_1 values are significantly higher than present CBG reservoir temperatures and the temperatures of typical microbial CBG formation temperatures (<80°C) (Fig.11). The calculated T_3 values (<5°C) are significantly lower than the CBG reservoir temperatures and the temperatures of typical microbial CBG formation. The calculated T_4 value is inconsistent with the CBG reservoir temperature. However, the T_2 values are close to the reservoir

497 temperatures for some samples (Fig.11). These results indicate that CH_4, CO_2
498 and HCO_3^- are isotopically in disequilibrium at present reservoir conditions in
499 the Fuxin Basin. However, the CH_4 and H_2O may be close to hydrogen isotope
500 equilibrium for some samples.
501 Applying a large dataset (n>500), Turner et al. (2021) found that microbial
502 CH_4 is in near isotopic equilibrium with co-occurring CO_2 and H_2O in some
503 CBG samples. For CBG and water samples in the Fuxin Basin, due to high
504 dissolution effect of CO_2, given most of the CO_2 formed in present reservoir
505 conditions have dissolved into coalbed water to form DIC and the amount of gas
506 CO_2 is too small to be neglected (CH_4/CO_2 are from 186 to 776), thus, the
507 $\delta^{13}C_{DIC}$ value is close to the $\delta^{13}C$ value of gaseous and dissolved CO_2. We used
508 $\delta^{13}C_{DIC}$ (instead of $\delta^{13}C_{CO2}$) and $\delta^{13}C_1$ to calculate the equilibrium temperature
509 T_5 of the reaction (6). The calculated T_5 (39 to 60°C) are consistent with the
510 CBG reservoir temperature (Fig. 11, Table 4). This result suggests that CH_4 and
511 CO_2 may be near isotopic equilibrium in their formation stage. However, high
512 CO_2 dissolution effect, associated with strong hydrodynamic activity in coalbed
513 aquifers, have led to isotopic kinetic fractionation of CO_2, causing the CH_4 and
514 CO_2 in present coalbeds are isotopically in disequilibrium. Overall, the kinetic
515 processes largely control isotopic compositions of the CBG and coalbed water in
516 the Fuxin Basin.
517
518 4.5 Origin and accumulation model of CBG in the Fuxin Basin
519 For microbial CBG, primary microbial CBG is generated in the early stage of
520 coalification. However, the upper limit of Ro of the source coal for primary microbial
521 CBG is not clear. The term ‘‘secondary biogenic (microbial) CBG’’ was introduced by

Scott et al. (1994) in the study of CBG in the San Juan Basin. Scott et al (1994) proposed that primary microbial CBG was not retained in the coal in significant quantities, most of microbial CBG found in coalbeds were secondary microbial gases. Strąpoć et al. (2011) distinguished microbial CBG from low-rank and high-rank coals. They suggested that microbial CBG from high-rank coalbeds was secondary microbial gas. These high-rank coalbeds had been buried at depths where the geothermal gradient could cause heat sterilization of coals. However, subsequent uplift to near surface would allow re-inoculation of these coalbeds with methanogenic microbial consortia via meteoric water recharge, thus, secondary microbial CBG can be generated. Numerous examples include CBG from the San Juan Basin (Scott et al., 1994), the Xinji area in China (Tao et al. 2007), and the Ningdong coalfield (Tao et al., 2021), and the Illinois Basin (Schlegel et al., 2011). However, for microbial CBG from low-rank coalbeds, researchers have not further distinguished primary and secondary microbial CBG. Examples included the CBG from subbituminous coalbeds in the Powder River Basin (Bates et al., 2011), and the CBG from the Cesar Rancheria Basin with Ro between 0.39 and 0.53% (Castaneda et al., 2022). We propose that secondary microbial CBG is the microbial gas formed after thermogenic CBG formation due to basin uplift and meteoric water recharge. Microbial CBG formed before thermogenic CBG formation is primary microbial gas.

According to the analysis of geochemical compositions of gas and water samples, the CBG in the Fuxin Basin is mainly microbial in origin (thermogenic gas cannot be identified). The low coal rank (Ro 0.4-0.6%) suggests that the Fuxin coalbeds are never buried deep enough to become temperature sterilized. Due to shallow depth and low temperature of coalbeds, the methanogenic microbial consortia *in situ* coalbeds may have been active, and extraneous microbial consortia may also enter coalbeds via

547 groundwater recharge. The microbial CBG probably has been continuously generated
548 since the deposition of the K_{1f} formation (113-107Ma). The Yanshan movement led to
549 uplift of the Fuxin Basin (~100Ma). During basin uplift, a portion of CBG may have
550 been lost. However, the uplift of K_{1f} coalbed aquifers to near surface allows re-
551 inoculation of coalbeds with methanogenic microbial consortia via meteoric water
552 recharge, which can accelerate the formation and accumulation of microbial CBG. As
553 a result, most of CBG in present coalbeds is likely generated after the uplift of coal
554 strata.
555

556 ## 5. Conclusions

557

558 The isotopic composition and distribution characteristics of gas and water in the
559 Fuxin Basin, associated with high $C_1/(C_2 + C_3)$ ratios > 1000 and low coal rank (Ro
560 0.4-0.6%), suggest that the Fuxin CBG is mainly microbial gas. The coalbed waters
561 are mainly from the meteoric water recharge. However, their isotope values may have
562 been modified by methanogenesis and water-rock interaction. The Na-HCO_3-Cl type
563 of water in the coalbed is favorable for methanogenesis. Although $\alpha_{CO2\text{-}C1}$ and $\Delta D_{H2O\text{-}}$
564 $_{CH4}$ indicators are inconsistent in distinguishing methanogenic pathways for the CBG
565 in the basin, CO_2 reduction is likely the dominated methanogenic pathway according
566 to $\Delta D_{H2O\text{-}CH4}$ indicator. Because this inconsistency may be mainly due to low $\delta^{13}C_{CO2}$
567 values and thus low $\alpha_{CO2\text{-}C1}$ values caused by high dissolution effect of CO_2 and
568 strong hydrodynamic activity in the Fuxin coalbed aquifers. CH_4, CO_2 and HCO_3^- are
569 isotopically in disequilibrium at present CBG reservoir conditions. However, CH_4 and
570 H_2O may be close to hydrogen isotope equilibrium for some CBG. Overall, kinetic
571 processes largely control isotopic compositions of the Fuxin CBG and coalbed water.

Most CBG in present coalbeds is likely generated after the uplift of coal strata in the Fuxin Basin, because the CBG formed before the basin uplift may have been lost during the uplift process. However, uplift to near surface would allow re-inoculation of coalbeds with methanogenic microbial consortia via meteoric water recharge, which can accelerate the formation and accumulation of microbial CBG.

Author Contributions

X.C. and Y.W. designed this research project. X.C., K.S. and Z.H. collected and analyzed samples. X.C., Y.W. and Z.Z. interpreted the data and wrote the paper. M.T. made significant contribution in data interpretation and discussion.

Declaration of competing interest

The authors declare that they have no known competing financial interests or personal relationships that could have appeared to influence the work reported in this paper.

Acknowledgments

We thank Lin Zhu, Qiang Wang and Jian Chen for their assistances in sample collection and measurement. Thanks to Liaoning Energy Geological Exploration & Development Research Institute Co.. Special thanks to anonymous reviewers for their important comments and suggestions. This research was funded by the Project of Stable Support for Youth Team in Basic Research Field, CAS (YSBR-017), the Strategic Priority Research Program of the Chinese Academy of Sciences (XDA14010103), the China Postdoctoral Science Foundation (2021M703223), and National Natural Science Foundation of China (41772122).

References

Akinfiev, N.N., Diamond, L.W., 2010. Thermodynamic model of aqueous CO_2–H_2O–NaCl solutions from -22 to 100°C and from 0.1 to 100 MPa. Fluid Phase Equilibr. 295, 104–124.

Aravena, R., Harrison, S.M., Barker, J.F., Abercrombie, H., Rudolph, D., 2003. Origin of methane in the Elk Valley coalfield, southeastern British Columbia, Canada. Chem. Geol. 195, 219–227.

Bates, B.L., McIntosh, J.C., Lohse, K.A., Brooks, P.D., 2011. Influence of groundwater flowpaths, residence times and nutrients on the extent of microbial methanogenesis in coal beds: Powder River Basin, USA. Chem Geol. 284, 45–61.

Baublys, K.A., Hamilton, S.K., Golding, S.D., Vink, S., Esterle, J., 2015. Microbial controls on the origin and evolution of coal seam gases and production waters of the Walloon Subgroup; Surat Basin, Australia. Int. J. Coal Geol. 147, 85–104.

Chen, J., Liu, D., Hou, X., Fan, Y., Jia, W., Zhang, B., Xiao, Z., 2018. Origin and evolution of oilfield waters in the Tazhong oilfield, Tarim Basin, China, and their relationship to multiple hydrocarbon charging events. Mar. Petrol. Geol. 98, 554–568.

Chen, X., Tao, M., Zhou, Z., Li, D., 2019. A new theoretical calculation of the equilibrium constant and temperature for the carbon isotope exchange reaction between CH_4 and CO_2. Geothermics 79, 140–144.

Chung, H.M., Gormly, J.R., Squires, R.M., 1988. Origin of gaseous hvdrocarbons in subsurface environment: theoretical considerations of carbon isotope distribution. Chem. Geol. 71, 97–104.

Clayton, R.N., Friedman, I., Graf, D.L., Mayeda, T.K., Meents,W.F., Shimp, N.F., 1966. Origin of saline formation water. 1. Isotopic composition. J. Geophys. Res. 71, 3869–3882.

Dai, J., 2018. Coal-derived gas theory and its discrimination. Chin Sci Bull, 63, 1291–1305 (in Chinese).

Duan, Z., Møller, N., Greenberg, J., Weare, J. H., 1992. The prediction of methane solubility

623 in natural waters to high ionic strength from 0 to 250°C and from 0 to 1600 bar. Geochim.
624 Cosmochim. Acta 56, 1451–1460.
625 Flores, R.M., Rice, C.A., Stricker, G.D., Warden, A., Ellis, M.S., 2008. Methanogenic
626 pathways of coal-bed gas in the Powder River Basin, United States: The geologic factor.
627 Int. J. Coal Geol. 76, 52–75.
628 Gaillardet, J., Dupré, B., Louvat, P., Allegre, C. J., 1999. Global silicate weathering and CO_2
629 consumption rates deduced from the chemistry of large rivers. Chem. Geol. 159, 3–30.
630 Gilfillan, S.M., Lollar, B.S., Holland, G., Blagburn, D., Stevens, S., Schoell, M., et al., 2009.
631 Solubility trapping in formation water as dominant CO2 sink in natural gas fields. Nature
632 458, 614–618.
633 Golding, S.D., Boreham, C.J., Esterle, J.S., 2013. Stable isotope geochemistry of coal bed and
634 shale gas and related production waters: A review. Int. J. Coal Geol. 120, 24–40.
635 Hamawand, I., Yusaf, T., Hamawand, S.G., 2013. Coal seam gas and associated water: a
636 review paper. Renew. Sust. Energ. Rev. 22, 550–560.
637 Hamilton, S.K., Golding, S.D., Baublys, K.A., Esterle, J.S., 2014. Stable isotopic and
638 molecular composition of desorbed coal seam gases from the Walloon Subgroup, eastern
639 Surat Basin, Australia. Int. J. Coal Geol. 122, 21–36.
640 Horita, J., 2001. Carbon isotope exchange in the system CO_2–CH_4 at elevated temperatures.
641 Geochim. Cosmochim. Acta 65, 1907–1919.
642 Harrison, S.M., Gentzis, T., Labute, G., Seifert, S., Payne, M., 2006. Preliminary
643 hydrogeological assessment of Late Cretaceous-Tertiary Ardley coals in part of the
644 Alberta Basin, Alberta, Canada. Int. J. Coal Geol. 65, 59–78.
645 Jia, J., Wu, Y., Miao, C., Fu, C., Xie, W., Qin, J., Wang, X. 2021. Tectonic controls on the
646 sedimentation and thermal history of supra-detachment basins: A case study of the early
647 cretaceous Fuxin basin, NE China. Tectonics, 40,1–26.
648 Kinnon, E.C.P., Golding, S.D., Boreham, C.J., Baublys, K.A., Esterle, J.S., 2010. Stable
649 isotope and water quality analysis of coal bed methane production waters and gases from
650 the Bowen Basin, Australia. Int. J. Coal Geol. 82, 219–231.

651 Kueter, N., Schmidt, M.W., Lilley, M.D., Bernasconi, S.M., 2019. Experimental
652 determination of equilibrium CH_4–CO_2–CO carbon isotope fractionation factors (300–
653 1200°C). Earth Planet. Sci. Lett. 506, 64–75.
654 Li, Q., Ju, Y., Bao, Y., Yan, Z., Li, X., Sun, Y., 2015. Composition, origin, and distribution of
655 coalbed methane in the Huaibei Coalfield, China. Energy Fuels, 29, 546–555.
656 Li, Q., Ju, Y., Lu, W., Wang, G., Neupane, B., & Sun, Y., 2016. Water-rock interaction and
657 methanogenesis in formation water in the southeast Huaibei coalfield, China. Mar. Petrol.
658 Geol. 77, 435–447.
659 Li, Z. Tao, M., Li, L., Wang, Z., Du, L., Zhang, M., 2007. Determination of isotope composition
660 of dissolved inorganic carbon by gas chromatography-conventional isotope-ratio mass
661 spectrometry. Chin. J. Anal Chem. 35, 1455–1458.
662 Lico, M.S., Kharaka, Y.K., Carothers, W.W., Wright, V.A., 1982. Methods for collection and
663 analysis of geopressured geothermal and oil field waters: United States, Geological Survey
664 Water Supply Paper 2194, 24 p, doi: 10.2172/5407477.
665 Liu, Q., Wu, X., Wang, X., Jin, Z., Zhu, D., Meng, Q., Huang, S., Liu, J., Fu, Q., 2019. Carbon
666 and hydrogen isotopes of methane, ethane, and propane: A review of genetic identification
667 of natural gas. Earth-Sci. Rev. 190, 247–272.
668 Lloyd, M.K., Trembath-Reichert, E., Dawson, K.S., Feakins, S.J., Mastalerz, M., Orphan, V.J.,
669 et al., 2021. Methoxyl stable isotopic constraints on the origins and limits of coal-bed
670 methane. Science 374, 894–897.
671 Mao, S., Zhang, D., Li, Y., Liu, N., 2013. An improved model for calculating CO_2 solubility in
672 aqueous NaCl solutions and the application to CO_2-H_2O-NaCl fluid inclusions. Chem.
673 Geol. 347, 43-58.
674 Martini, A.M.,Walter, L.M., Ku, T.C.W., Budai, J.M., McIntosh, J.C., Schoell, M., 2003.
675 Microbial production and modification of gases in sedimentary basins: a geochemical case
676 study from a Devonian shale gas play, Michigan Basin. AAPG Bull. 87, 1355–1375.
677 Mayumi, D., Mochimaru, H., Tamaki, H., Yamamoto, K., Yoshioka, H., Suzuki, Y.,
678 Kamagata, Y., Sakata, S., 2016. Methane production from coal by a single methanogen.

679 Science 354, 222–225.
680 Meng, Y., Tang, D., Xu, H., Li, Y., Gao, L., 2014. Coalbed methane produced water in China:
681 status and environmental issues. Environ. Sci. Pollut. Res. 21, 6964–6974.
682 Milkov, A.V., Etiope, G., 2018. Revised genetic diagrams for natural gases based on a global
683 dataset of >20,000 samples. Org. Geochem. **125,** 109–120.
684 Mitterer, R.M., 2010. Methanogenesis and sulfate reduction in marine sediments: a new model.
685 Earth Planet. Sci. Lett. 295, 358–366.
686 Mook, W.G., Bommerson, J.C. and Staverman, W.H. (1974) Carbon isotope fractionation
687 between dissolved bicarbonate and gaseous carbon dioxide. Earth Planet. Sci. Lett. 22,
688 169–176.
689 Park, S.Y., Liang, Y., 2016. Biogenic methane production from coal: A review on recent
690 research and development on microbially enhanced coalbed methane (MECBM). Fuel
691 166, 258–267.
692 Rathi, R., Lavania, M., Singh, N., Sarma, P. M., Kishore, P., Hajra, P., Lal, B., 2019.
693 Evaluating indigenous diversity and its potential for microbial methane generation from
694 thermogenic coal bed methane reservoir. Fuel, 250, 362–372.
695 Richet, P, Bottinga, Y., Javoy, M.A., 1977. Review of Hydrogen, Carbon, Nitrogen, Oxygen,
696 Sulphur, and Chlorine Stable Isotope Fractionation Among Gaseous Molecules. Annu. Rev.
697 Earth Planet. Sci. 5, 65–110.
698 Rice, D.D., Claypool, G.E., 1981. Generation, accumulation, and resource potential of biogenic
699 gas. AAPG Bull. 65, 5–25.
700 Schlegel, M.E., McIntosh, J.C., Bates, B.L., Kirk, M.F., Martini, A.M., 2011. Comparison of
701 fluid geochemistry and microbiology of multiple organic–rich reservoirs in the Illinois
702 Basin, USA: evidence for controls on methanogenesis and microbial transport. Geochim.
703 Cosmochim. Acta 75, 1903–1919.
704 Schoell, M., 1980. The hydrogen and carbon isotopic composition of methane from natural
705 gases of various origins. Geochim. Cosmochim. Acta 44, 649–661.
706 Scott, A.R., Kaiser, W.R., Ayers Jr., W.B., 1994. Thermogenic and secondary biogenic gases,

San Juan basin, Colorado and New Mexico-implications for coalbed gas producibility. AAPG Bull. 78, 1186–1209.

Sepulveda-Castaneda, V. M., Esterle, J. S., Golding, S.D., Gonzalez, S., 2022. Isotopic and hydrogeochemical evidence for biogenic gas in Cuervos Formation coal beds, Cesar Rancheria Basin, Colombia. Int. J. Coal Geol. 249, 103882.

Sharma, S., Baggett, J.K., 2011. Application of carbon isotopes to detect seepage out of coalbed natural gas produced water impoundments. Appl. Geochem. 26, 1423–1432.

Stolper, D., Lawson, M., Davis, C.L., Ferreira, A.A., Neto E.V.S., et al., 2014. Formation temperatures of thermogenic and biogenic methane. Science 344, 1500–1503.

Strąpoć, D., Mastalerz, M., Dawson, K., Macalady, J., Callaghan, A.V., Wawrik, B., Turich, C., Ashby, M., 2011. Biogeochemistry of microbial coal–bed methane. Ann. Rev. Earth Planet. Sci. 39, 617–656.

Strąpoć, D., Mastalerz, M., Eble, C., Schimmelmann, A., 2007. Characterization of the origin of coalbed gases in southeastern Illinois Basin by compound-specific carbon and hydrogen stable isotope ratios. Org. Geochem. 38, 267–287.

Tao, M., Chen, X., Li, Z., Ma, Y., Xie, G., Wang, Y., et al., 2021. Variation characteristic and mechanism of carbon isotope composition of coalbed methane under different conditions and its tracing significance. Fuel 302, 1–9.

Tao, M., Chen, X., Ma, Y., Wang, Y., Li, Z., Xiao, W., Huang, Z., 2020. Geological-geochemical models and isotope fractionation laws and control factors of thermogenic coalbed gas in Panxian, China. Energy Fuel 34, 2665–2673.

Tao, M., Ma, Y., Li, Z., Li, J., Liu, P., Wang, Y., Chen, X., et al., 2015. The isotopic tracer and resource value of microbial gas production in coalbeds-a case study of coalbed gas in Enhong, China. Energy Fuel 29, 2134–2142.

Tao, M., Shi, B., Li, J., Wang, W., Li, X., Gao, B., 2007. Secondary biological coalbed gas in the Xinji area, Anhui province, China: evidence from the geochemical features and secondary changes. Int. J. Coal Geol. 71, 358–370.

Taylor Jr., H.P., 1997. Oxygen and hydrogen isotope relationships in hydrothermal mineral

735 deposits, In: Barnes, H.L. (Ed.), Geochemistry of Hydrothermal Ore Deposits, 3rd ed.
736 John Wiley and Sons, New York, pp. 229–302.
737 Thiagarajan, N., Xie, H., Ponton, C., Kitchen, N., Peterson, B., Lawson, M., Formolo, M.,
738 Xiao, Y., Eiler, J., 2020. Isotopic evidence for quasi-equilibrium chemistry in thermally
739 mature natural gases. Proc. Natl. Acad. Sci. USA. 117, 3989–3995.
740 Turner, A.C., Korol, R., Eldridge, D.L., Bill, M., Conrad, M., Miller, T.F., Stolper, D.A., 2021.
741 Experimental and theoretical determinations of hydrogen isotopic equilibrium in the
742 system CH_4–H_2–H_2O from 3 to 200°C. Geochim. Cosmochim. Acta 314, 223–269.
743 Van Voast, W.A., 2003. Geochemical signature of formation waters associated with coalbed
744 methane. AAPG Bull. 87, 667–676.
745 Vinson, D.S., Blair, N.E., Martini, A.M., Larter, S., Orem, W.H., McIntosh, J.C., 2017.
746 Microbial methane from in situ biodegradation of coal and shale: A review and
747 reevaluation of hydrogen and carbon isotope signatures. Chem. Geol. 453,128–145.
748 Wang, D.T, Gruen, D.S., Lollar, B.S., Hinrichs, K.U., Stewart, L.C., et al., 2015.
749 Nonequilibrium clumped isotope signals in microbial methane. Science 348, 428–431.
750 Wang, X., Lu, A., Zhang, X., 2007. The features of oil- and gas-bearing strata in the Fuxin
751 Basin. J. Stratigr. 31, 385–390.
752 Wang, F., Sun, Q., Cai, B., Zhang, L., Li, M., Li, T., 2016. Variation of $\delta^{18}O$ in the meteoric
753 precipitation, drip water and their calcite deposition in Miaodong cave, Liaoning province
754 and its implications for palaeoclimatic reconstructions. Quaternary Sci, 36,1370-1382 (in
755 Chinese).
756 Whiticar, M.J., 1999. Carbon and hydrogen isotope systematics of bacterial formation and
757 oxidation of methane. Chem. Geol. 161, 291–314.
758 Whiticar, M.J., Faber, E., Schoell, M., 1986. Biogenic methane formation in marine and
759 freshwater environments: CO_2 reduction vs acetate fermentation–isotope evidence.
760 Geochim. Cosmochim. Acta 50, 693–709.
761 Xiao, D., Peng, S., Wang, B., Yan, X., 2013. Anthracite bio–degradation by methanogenic
762 consortia in Qinshui basin. Int. J. Coal Geol. 116, 46–52.

763 Xie, H., Dong, G., Formolo, M., Lawson, M., Liu, J., Cong, F., et al., 2021. The evolution of
764 intra– and inter–molecular isotope equilibria in natural gases with thermal maturation.
765 Geochim. Cosmochim. Acta 307, 22–41.
766 Xie, S., 2020. Reservoir characteristics and productivity of coalbed methane, Liujia mining
767 area, Fuxin Basin. Nat. Gas Explor. Dev. 43, 96–102 (in Chinese).
768 Xu, Z., Liu, Q., Zheng, Q., Cheng, H., Wu, Y., 2016. Isotopic composition and content of
769 coalbed methane production gases and waters in karstic collapse column area, Qinshui
770 Coalfield, China. J. Geochim. Explor. 165, 94–101.
771 Zhang, D., Zhao, H., Chen, S., Zhang, J., 2021. Lithostratigraphic characteristics of LFD-2
772 well in Fuxin Basin. Geol. Res. 30, 325–332 (in Chinese).
773 Zhang, J., Liang, Y., Pandey, R., & Harpalani, S., 2015. Characterizing microbial
774 communities dedicated for conversion of coal to methane in situ and ex situ. Int. J. Coal
775 Geol. 146, 145–154.
776 Zhou, Z., Ballentine, C.J., Kipfer, R., Schoell, M., Thibodeaux, S., 2005. Noble gas tracing of
777 groundwater/coalbed methane interaction in the San Juan Basin, USA. Geochim.
778 Cosmochim. Acta 69, 5413–5428.
779 Zhu, Z., Shen, B., Cui, H. Q., Zhou, J. Y., 2007. Genetic analysis of coal-bed methane in
780 Fuxin Basin. Geol. Sci. Technol. Infor. 3, 67–70 (in Chinese).

Figs. 1-11

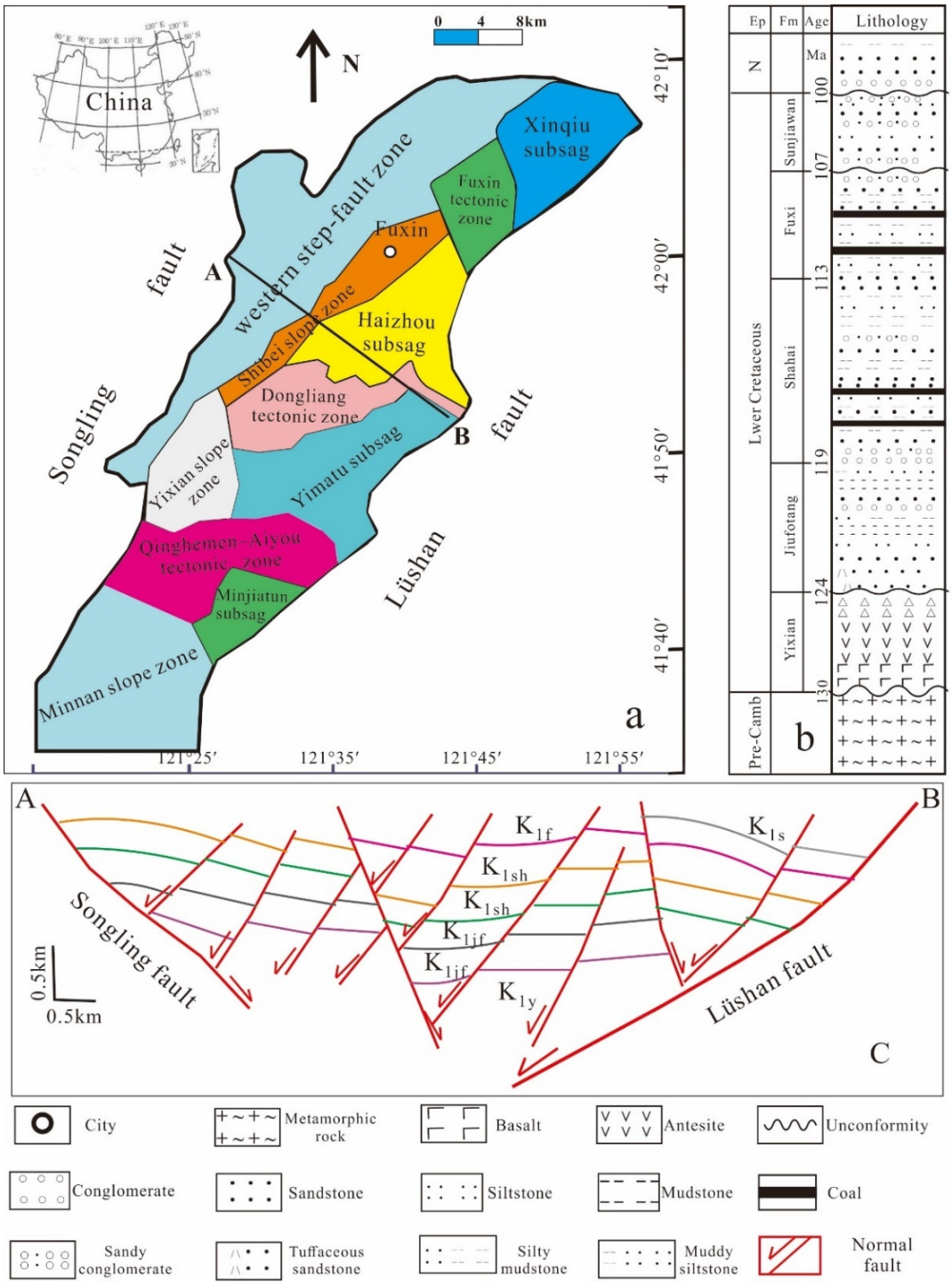

Fig. 1. (a) Simplified tectonic map of the Fuxin Basin, China (after Jia et al., 2021). (b) Diagram of generalized strata column of the Fuxin Basin (after Jia et al., 2021 and Zhang et al., 2021). (c) Cross-section of the Fuxin Basin (after Jia et al., 2021). Abbreviations: Ep, epoch; N, Neogene; Pre-camb, Pre-cambrian; Fm, Formation. Our samples are from the Haizhou subsag.

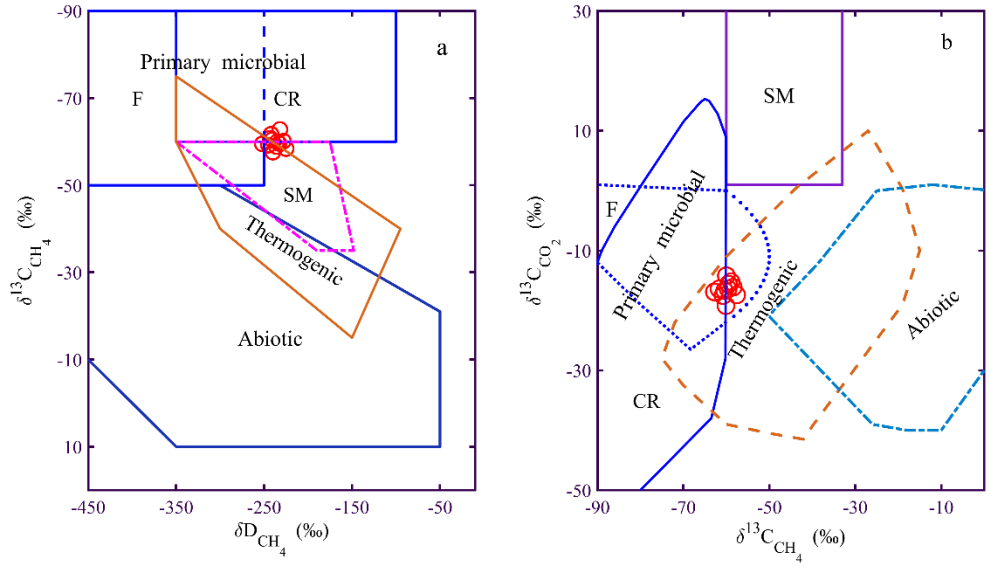

789

790 **Fig. 2.** (a) Genetic diagram of $\delta^{13}C_1$ vs. δD_{CH4} for our CBG samples (after Milkov and

791 Etiope, 2018). (b) Genetic diagram of $\delta^{13}C_{CO2}$ vs. $\delta^{13}C_1$ for our CBG samples (after

792 Milkov and Etiope, 2018). (F: methyl-type fermentation, CR: CO_2 reduction, SM:

793 secondary microbial).

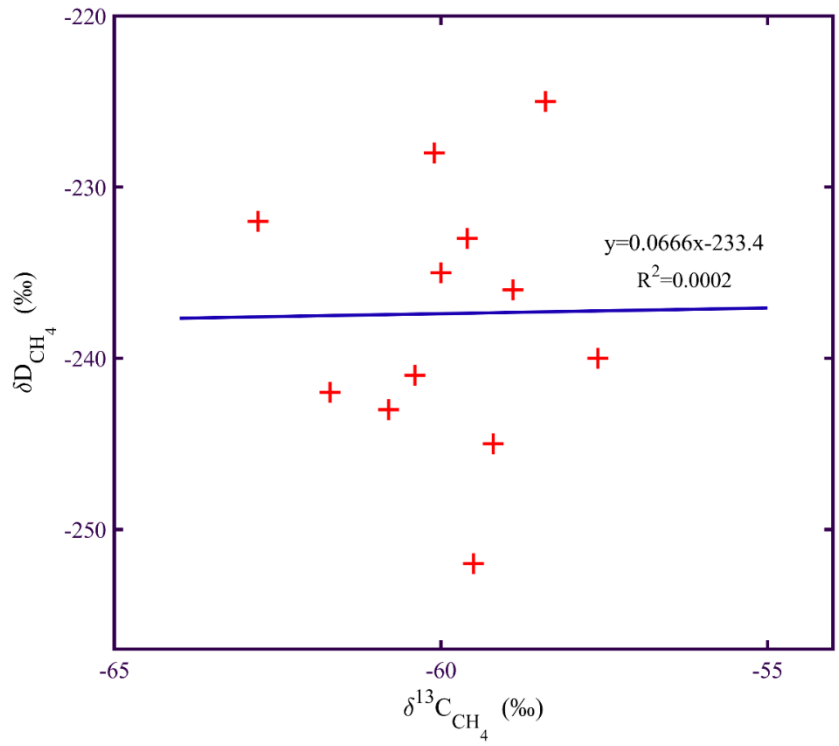

794

795 **Fig. 3.** The relationship of $\delta^{13}C_1$ vs. δD_{CH4} for Fuxin CBG samples. It reflects that

796 their correlation is extremely low.

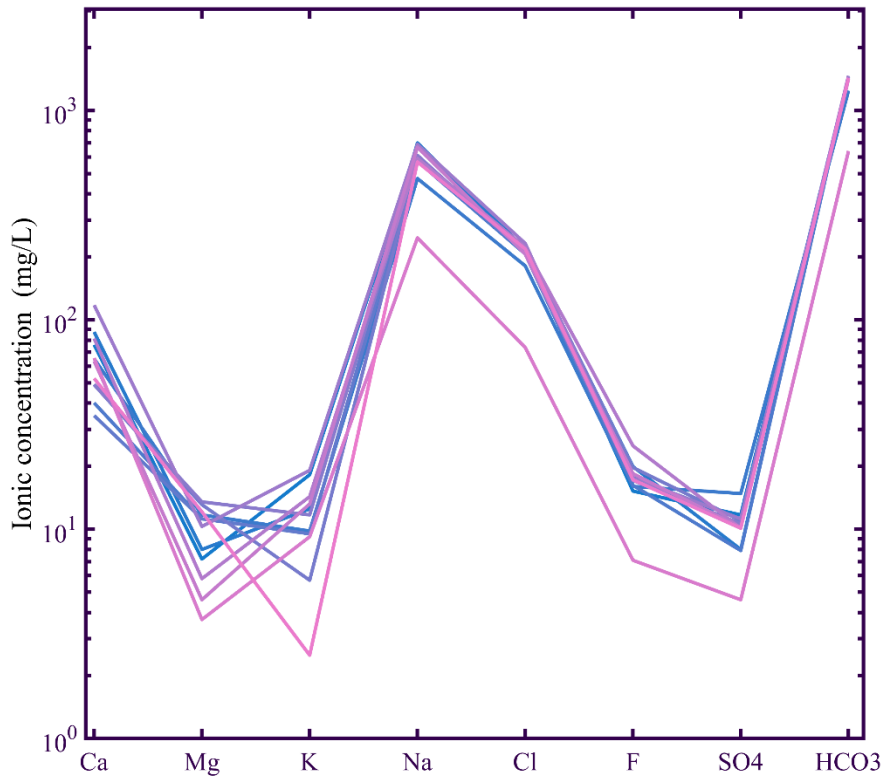

797

798 **Fig. 4.** Schoeller diagrams illustrating the chemical compositions of coalbed water

799 samples from the Fuxin Basin. It shows that the Fuxin coalbed water is Na-HCO_3-Cl

800 type water.

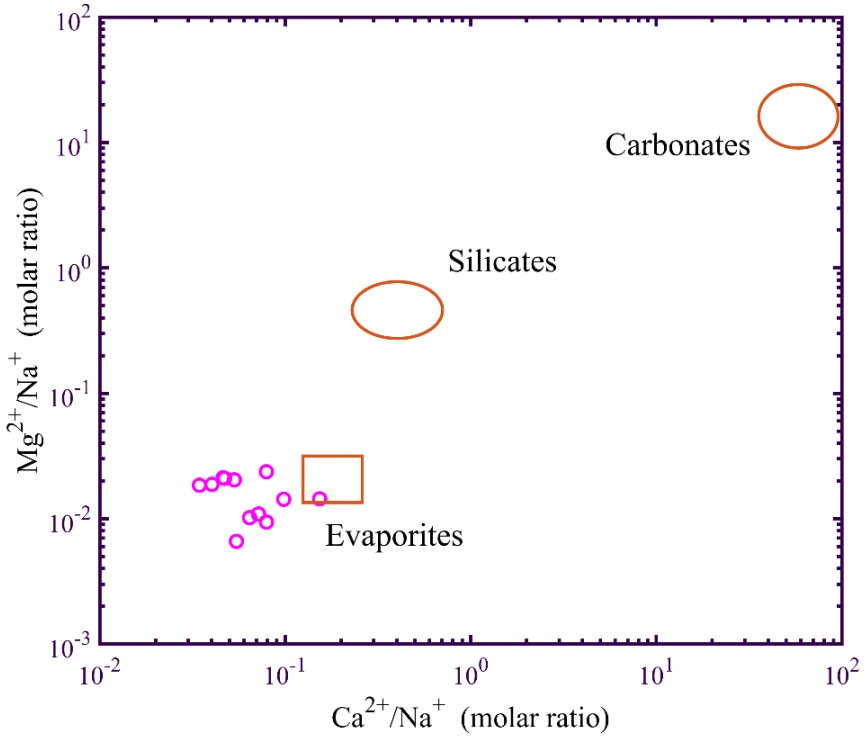

Fig. 5. Diagrams for distinguishing Ca^{2+} and Mg^{2+} sources in Fuxin coalbed water samples by using Na-normalized molar ratios of Mg^{2+} and Ca^{2+} (after Gaillardet et al., 1999 and Li et al., 2016). It shows that Ca and Mg cations in the water samples mainly originate from the dissolution of evaporites.

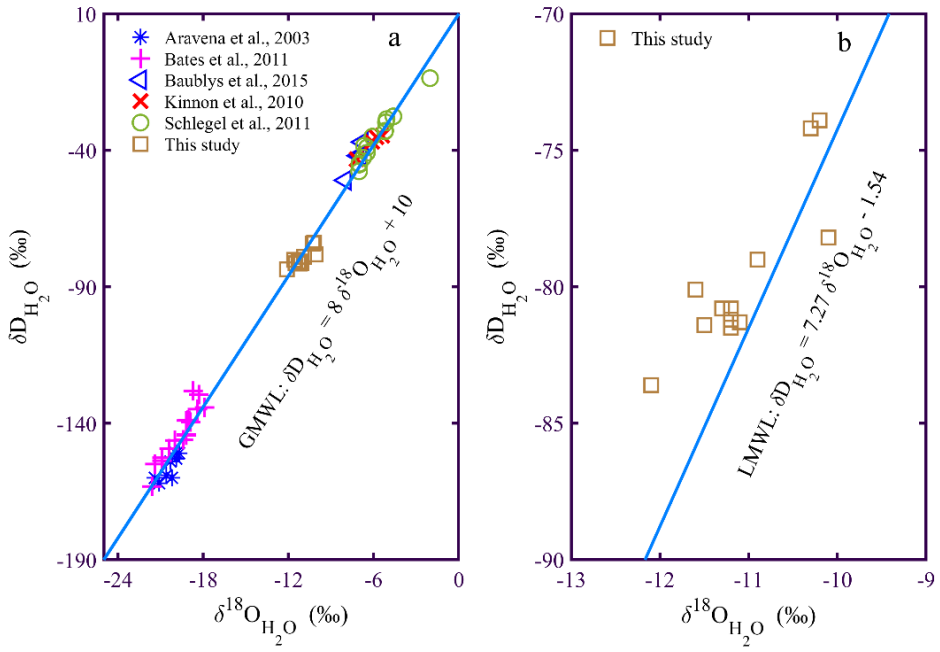

Fig. 6. Plot of δD_{H2O} vs. $\delta^{18}O_{H2O}$ for coalbed water samples. (a) Samples from the Fuxin Basin, the Elk Valley coalfield (Aravena et al., 2003), the Bowen Basin (Kinnon et al., 2010), the Powder River Basin (Bates et al., 2011), the Illinois Basin (Schlegel et al., 2011), and the Surat Basin (average, Baublys et al., 2015). (b) Samples from the Fuxin Basin. GMWL: global meteoric water line. LMWL: local meteoric water line.

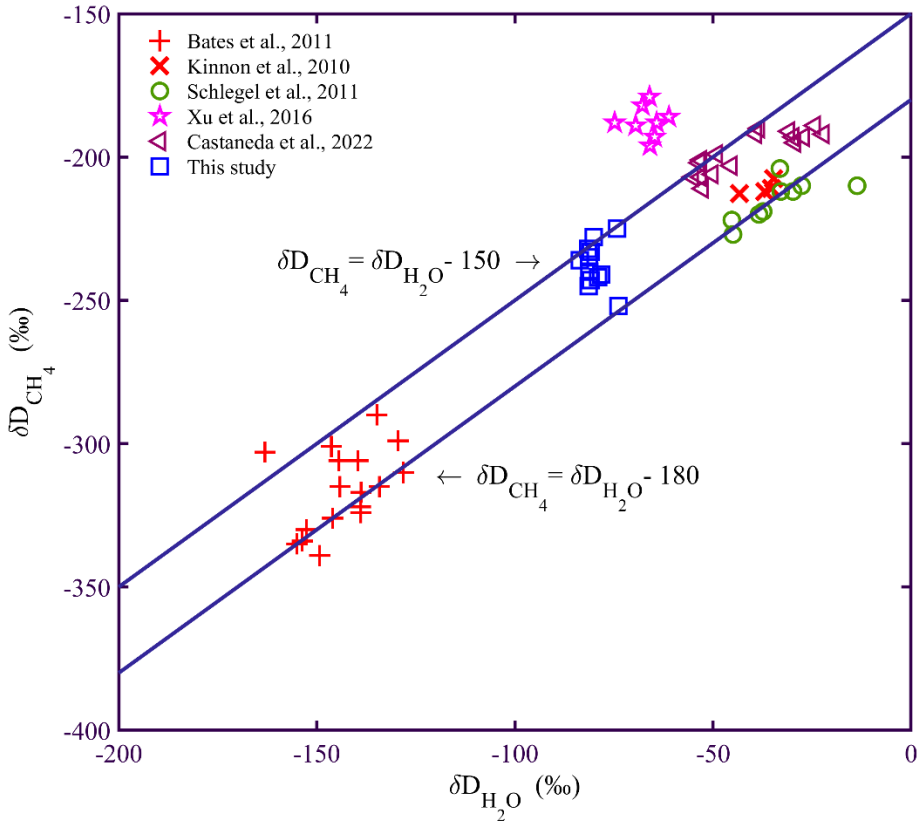

Fig. 7. Plot of δD_{CH4} vs. δD_{H2O} for CBG and coproduction water samples from various studies, including the Powder River Basin (Bates et al., 2011), the Bowen Basin (Kinnon et al., 2010), the Illinois Basin (Schlegel et al., 2011), the Cesar Rancheria Basin (Castaneda et al., 2022), and the Qinshui Basin (Xu et al., 2016).

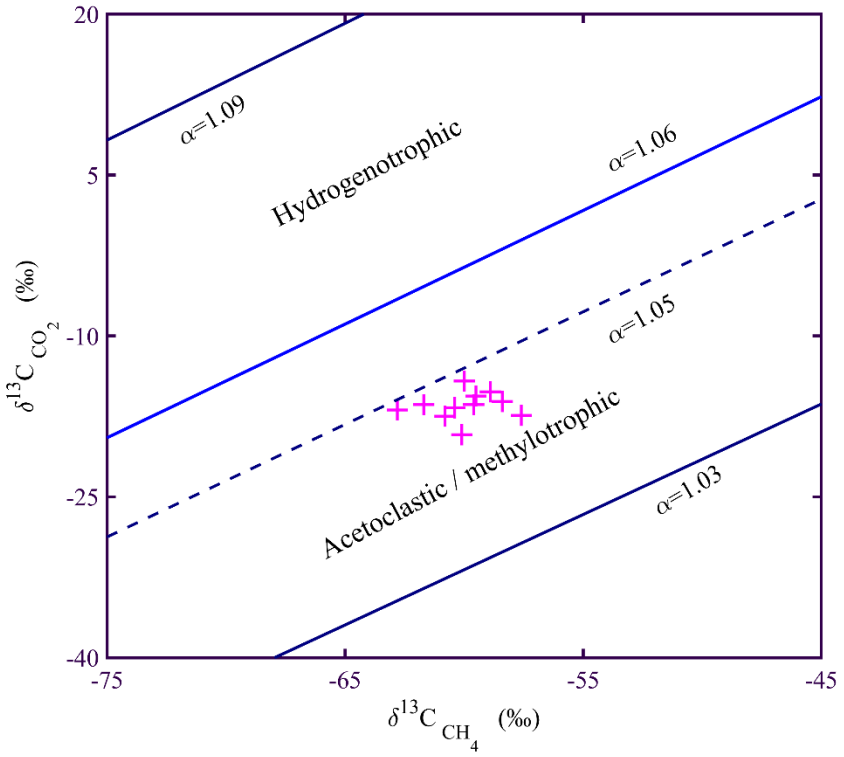

818

819 **Fig. 8.** (a) Plot of $\delta^{13}C_{CO2}$ vs. $\delta^{13}C_1$ for Fuxin CBG samples. In general, $\alpha_{CO2\text{-}C1}$ values

820 for CO_2 reduction and methyl-type fermentation range from 1.06 (or 1.05) to 1.09, and

821 1.03 to 1.06, respectively.

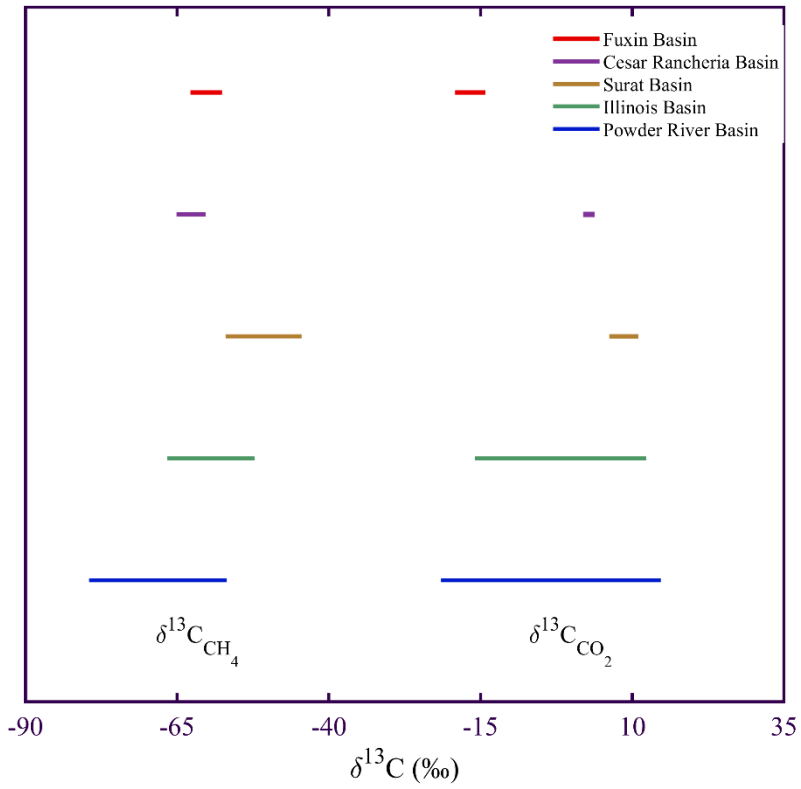

822

823 **Fig. 9.** Comparation of $\delta^{13}C_1$ and $\delta^{13}C_{CO2}$ values in microbial CBG from different
824 basins. Data are from the Powder River Basin (Bates et al., 2011), the Illinois Basin
825 (Schlegel et al., 2011), the Surat Basin (Baublys et al., 2015), the Cesar Rancheria
826 Basin (Castaneda et al., 2022), and the Fuxin Basin in this study. It shows that the
827 $\delta^{13}C_1$ values of Fuxin samples are consistent with the $\delta^{13}C_1$ values from other CBG
828 basins. However, the $\delta^{13}C_{CO2}$ values of Fuxin samples are significantly lower than the
829 $\delta^{13}C_{CO2}$ values from other basins.

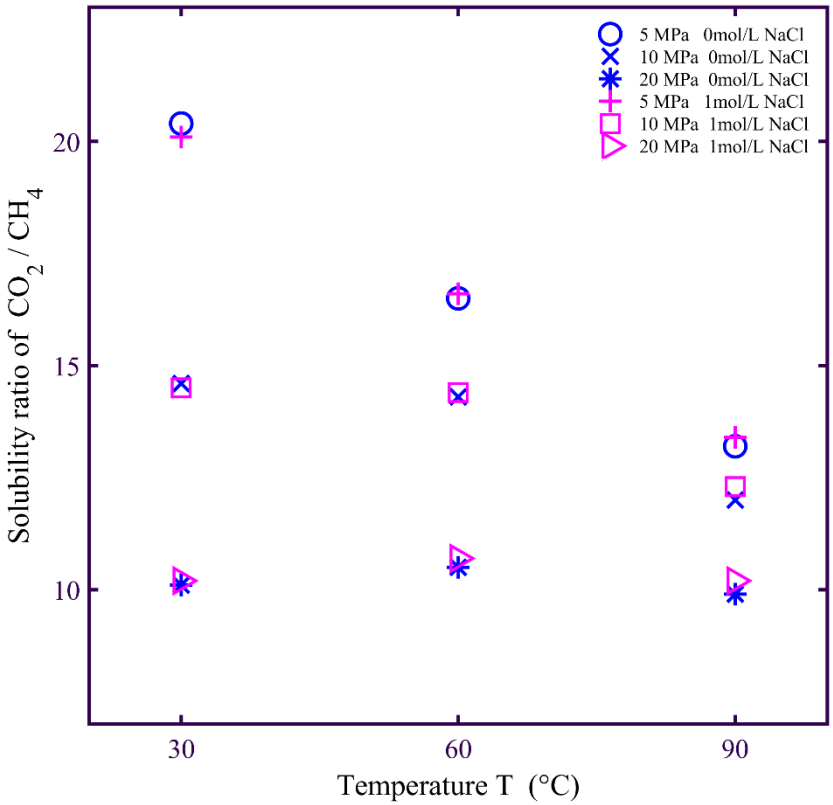

830

831 **Fig. 10.** The solubility ratios of CO_2 and CH_4 in water under various temperature,

832 pressure and salinity conditions. The solubility of CO_2 can be more than 10 times than

833 that of CH_4 under certain conditions. The data are from Duan et al. (1992) and

834 Akinfiev and Diamond (2010).

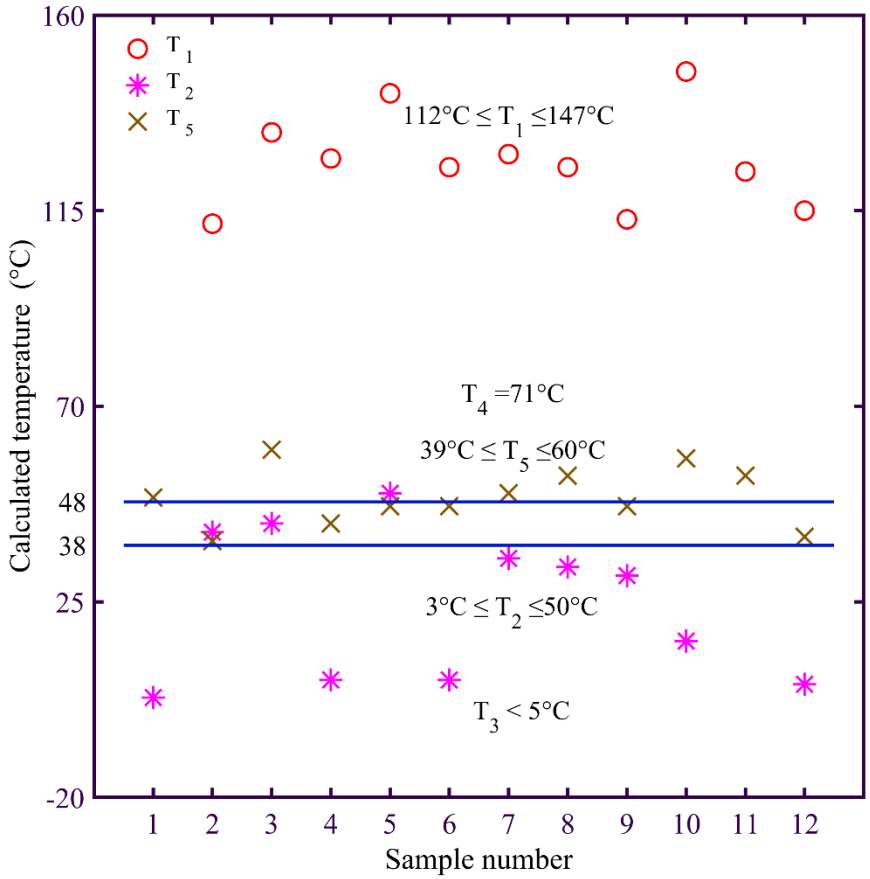

Fig. 11. Comparation of the calculated equilibrium temperatures T_1-T_5 and the reservoir temperatures of Fuxin CBG samples. The reservoir temperatures are between 38°C and 48°C. T_1, T_3 and T_4 are significantly different from the reservoir temperatures. T_2 and T_5 are consistent with the reservoir temperatures for some samples.

Tables 1-4

Table 1.

Molecular and isotope compositions of gas and water samples from the CBG production wells in the Fuxin Basin

Sample code	Gas composition (%)			Isotope value (‰)							
	CH_4	CO_2	N_2	$\delta^{13}C_1$	δD_{CH4}	$\delta^{13}C_{CO2}$	$\delta^{13}C_{DIC}$	δD_{H2O}	$\delta^{18}O_{H2O}$	$\Delta D_{H2O-CH4}$	α_{CO2-C1}
FX-1	91.93	0.39	7.68	-59.2	-245	-	1.43	-81.4	-11.5	163.6	-
FX-2	93.18	0.12	6.62	-62.8	-232	-16.9	0.75	-81.5	-11.2	150.5	1.05
FX-3	93.58	0.20	6.22	-58.4	-225	-16.1	-0.59	-74.2	-10.3	150.8	1.04
FX-4	93.11	0.50	6.39	-60.8	-243	-17.5	1.62	-80.8	-11.2	162.2	1.05
FX-5	94.14	0.27	5.58	-60.1	-228	-19.2	1.07	-80.1	-11.6	147.9	1.04
FX-6	93.40	0.26	6.34	-60.4	-241	-16.7	0.9	-78.2	-10.1	162.8	1.05
FX-7	93.18	0.25	6.57	-59.6	-233	-16.4	0.78	-80.8	-11.3	152.2	1.05
FX-8	92.98	0.39	6.63	-58.9	-236	-15.2	0.34	-83.6	-12.1	152.4	1.05
FX-9	93.67	0.25	6.08	-60	-235	-14.2	1.26	-81.3	-11.1	153.7	1.05
FX-10	93.05	0.18	6.77	-57.6	-240	-17.4	0.73	-81.2	-11.2	158.8	1.04
FX-11	93.17	0.27	6.56	-59.5	-252	-15.6	-0.06	-73.9	-10.2	178.1	1.05
FX-12	94.51	0.29	5.20	-61.7	-242	-16.4	1.54	-79.0	-10.9	163.0	1.05

“-” denote that the data is not measured.

847 **Table 2.**

848 Chemical components of coalbed water samples from the Fuxin Basin

Sample code	pH	TDS mg/L	Alkalinity as HCO_3^-	Ion concentration (mg/L)						
				F^-	Cl^-	SO_4^{2-}	Na^+	K^+	Mg^{2+}	Ca^{2+}
FX-1	8.46	1392.5	1451.8	15.2	211.7	11.7	679.7	18.2	7.2	76.0
FX-2	8.38	1355.0	1464.0	19.9	217.6	8.0	700.3	12.5	8.0	87.5
FX-3	8.38	1195.0	1244.4	16.0	181.1	14.8	473.4	9.8	11.7	65.2
FX-4	8.31	1417.5	1439.6	16.2	206.3	7.9	571.8	9.5	11.2	40.1
FX-5	8.38	1362.5	1445.7	17.6	219.4	11.2	580.9	9.5	11.2	34.9
FX-6	8.41	1390.0	1439.6	19.7	219.5	11.0	597.8	5.7	13.1	49.0
FX-7	8.40	1400.0	1451.8	17.1	208.8	10.6	610.7	11.7	13.5	49.2
FX-8	8.33	1390.0	1464.0	17.5	231.8	11.2	688.9	19.1	10.3	117.6
FX-9	8.42	1362.5	1415.2	25.0	222.0	10.1	590.2	14.3	5.8	81.4
FX-10	8.31	1400.0	1415.2	18.4	206.0	10.2	668.2	13.2	4.6	63.5
FX-11	8.08	545.0	640.5	7.1	73.8	4.6	246.4	9.2	3.7	65.7
FX-12	8.34	1385.0	1433.5	17.2	218.1	10.1	567.9	2.5	12.1	52.5

849

Table 3.

The ranges of $\delta^{13}C$ of CH_4-CO_2-DIC and TDS concentrations in basins with microbial CBG.

Basin	Range (‰)				TDS	References
	$\delta^{13}C_1$	$\delta^{13}C_{CO2}$	$\delta^{13}C_{DIC}$	$\Delta D_{H2O-CH4}$	mg/L	
Fuxin	-62.8 to -57.6	-19.2 to -14.2	-0.1 to 1.6	148 to 178	545-1418	This study
Powder River	-79.5 to -56.8	-21.5 to 14.7	-12.7 to 24.1	147 to 190	457-4220	Bates et al. 2011
Illinois	-66.6 to -52.2	-15.9 to 12.3	-13.5 to 35.1	170 to 196	--	Schlegel et al. 2011
Surat	-57.0 to -44.5	6.2 to 11.0	1.2 to 25.9*	161 to 188	3627#	Baublys et al. 2015
Cesar Rancheria	-65.1 to -60.3	1.9 to 3.8	-0.9 to 9.7	148 to 170	2268-6602	Sepulveda et al. 2022

* Except for sample HM-12 with $\delta^{13}C_{DIC}$ of -10.8‰; # Average value

Table 4.

Isotopic differences of CH_4-CO_2-H_2O-DIC and calculated equilibrium temperatures

Sample code	Isotopic difference (‰)				*Temperature (°C)				
	$\Delta^{13}C_{CO2\text{-}C1}$	$\Delta D_{H2O\text{-}CH4}$	$\Delta^{13}C_{DIC\text{-}CO2}$	$\Delta^{13}C_{DIC\text{-}C1}$	T_1	T_2	T_3	T_4	T_5
FX-1	-	163.6	-	60.6	-	3	-		49
FX-2	45.9	150.5	17.7	63.6	112	41	<5		39
FX-3	42.3	150.8	15.5	57.8	133	43	<5		60
FX-4	43.3	162.2	19.1	62.4	127	7	<5		43
FX-5	40.9	147.9	20.3	61.2	142	50	<5		47
FX-6	43.7	162.8	17.6	61.3	125	7	<5	71	47
FX-7	43.2	152.2	17.2	60.4	128	35	<5		50
FX-8	43.7	152.4	15.5	59.2	125	33	<5		54
FX-9	45.8	153.7	15.5	61.3	113	31	<5		47
FX-10	40.2	158.8	18.1	58.3	147	16	<5		58
FX-11	43.9	178.1	15.5	59.4	124	<0	<5		54
FX-12	45.3	163.0	17.9	63.2	115	6	<5		40

"-" denote the data is not measured or calculated. The estimated reservoir temperatures are between 38°C and 48°C.

* The T_1, T_2, T_3 and T_5 are calculated by the $\delta^{13}C$ values of CH_4 and CO_2, the δD values of CH_4 and H_2O, the $\delta^{13}C$ values of DIC and CO_2, and $\delta^{13}C$ values of CH_4 and DIC, respectively. The T_4 is calculated by the average values of $\delta^{13}C_{DIC}$, $\delta^{13}C_{CH4}$ and CBG reservoir temperatures.